Title Rolled-up membranes from GaAs/AlOx core-shell nanowire ensembles through natural oxidation

Hidetoshi Hashimoto, Keisuke Minehisa, Kaito Nakama,*
*Kentaro Watanabe, Kazuki Nagashima, Takeshi Yanagida, Fumitaro Ishikawa**

H. Hashimoto, K. Minehisa, K. Nakama, and F. Ishikawa
Research Center for Integrated Quantum Electronics, Hokkaido University. North 13 West 8, Sapporo, 060-0813, Japan
E-mail: hashimoto.hidetoshi@rciqe.hokudai.ac.jp
E-mail: ishikawa.fumitao@rciqe.hokudai.ac.jp

K. Watanabe
Institute for Fiber Engineering and Science (IFES), Interdisciplinary Cluster for Cutting Edge Research (ICCER), Shinshu University. 3-15-1 Tokida, Ueda, Nagano, 386-8567, Japan

K. Nagashima
Research Institute for Electronic Science, Hokkaido University. North 21 West 10, Sapporo, 001-0021, Japan

T. Yanagida
School of Engineering, The University of Tokyo. 2-11-16 Yayoi, Bunkyo-ku, Tokyo, 113-0032, Japan

Keywords: nanowires, compound semiconductors, GaAs, oxide, rolled up membrane

We report the formation of rolled-up cylindrical membranes stemming from the strain deformation-induced delamination of a film-like nanowires array composed of coalesced GaAs nanowires embedded in AlOx with a buried GaAs/AlAs core-shell structure. The delamination of the nanowires array film is driven by natural oxidation resulting from prolongated exposure to ambient atmosphere. Investigation of the structural characteristics of the nanowires in the array reveal an analytical description of the oxidation mechanism leading to the formation of the rolled-up structures. The membrane can be easily transferred by simply

shaking off the surface membranes of the sample. The cylindrical membranes maintain the optical properties of the core GaAs nanowires surrounded by native oxide. Our findings show the prospects for area-saving and transferable semiconductor devices with advanced nanoscale optical functions.

1. Introduction

Rolled up microtubes have attracted great interest as owing to their high flexibility, integrability, and versatility[1-7] which can be used for a variety of device applications including sensors, batteries, and transistors, among many others.[3,6] Rolled up semiconductor membranes obtained by strain engineering are the materials of interest due to their advantages in terms of unique physical architecture and hybrid functionalization that allow the on-chip fabrication of complex architectures compared with the other three dimensional-patterned structures. [3,6,8,9] A representative example of a rolled-up microtube is a structure where InAs/GaAs heteroepitaxial layers, characterized by a significant lattice mismatch, are grown on a sacrificial AlAs layer. Upon selective etching of the AlAs sacrificial layer, the InAs/GaAs bilayer is released from the substrate, resulting in tube formation. This process is driven by the generation of a bending moment due to the compressive strain in the InAs layer and the tensile strain in the GaAs layer.[3] The synthesized membranes can be utilized for functional and small-size controlled electrical and optical semiconductor devices, such as inductors[10], or light emitting diodes having superior light emission and extraction efficiency because of the suppressed non-radiative recombination and preferably controlled electromagnetic wave distributions.[2,7,11] Further, those can be assembled, dispersed, and transferred to the desired substrate that allows the construction of on-chip integrated circuit components monolithically and reducing the footprint of the device drastically.[9,10,12] Besides, III–V compound semiconductor nanowires (NWs) as promising materials for various device applications in solid-state lighting, integrated nanophotonics, and nanoelectronics,[13-20] owing to their superior electrical, optical, and efficient energy conversion properties.[21-36] Oxidation processes in III–V semiconductors were shown particularly effective

for enhancing the performances of optical devices, as they introduce large contrasts in electron conductivity and refractive index, thereby confining charge carriers and light propagation.[23-37] Namely, the native oxidation of Al-rich AlGaAs has been popular in III–V semiconductors owing to its simple occurrence under ambient conditions.[38,39] Its electrical insulation and effective surface passivation functionalities have made it attractive for application in functional optical devices and AlGaAs-GaAs III–V heterostructures.[39-43] Consequently, the AlO_x obtained by the oxidation of AlGaAs has been utilized in the fabrication of edge-emitting lasers,[44] optical waveguides,[45] and GaAs metal-oxide-semiconductor field effect transistors.[42] To introduce those functions into the nanowires system, we have developed the controlled formation of $(Al,Ga)O_x$ oxide shells around GaAs nanowires cores involving wet or native oxidation of Al-rich AlGaAs. [38,46,47] Based on the above background, the synthesis of rolled up membranes that combine GaAs nanowires and AlO_x will open up prospects for area-saving semiconductor device integration with advancement optical functions. In the present study, we report the formation through natural oxidation of strain deformation-induced rolled-up cylindrical membranes composed of GaAs nanowires embedded in AlO_x with buried GaAs/Al-rich AlGaAs core-shell nanowires. In our approach, etching of a sacrificial layer is unnecessary, as the nanowires spontaneously fracture near their bases due to strain-induced forces.

2. Results and Discussion

We fabricated two series of GaAs/AlAs core-shell NW arrays, with different AlAs shell widths, on 2” Si(111) substrate wafers.[48] For the two NW array samples, we grew a top GaAs layer on the outermost surface to prevent drastically rapid oxidation of AlAs；the surface would be full of cracks without the GaAs layer. The density of the NWs in the arrays is about 8×10^7 cm^{-2}. The GaAs core NWs are ~5 μm in length and ~130 nm in diameter, with a different thickness of the AlAs shell layer, controlled by its growth time. For the thinner AlAs shell sample, the growth of AlAs over 1.5 h resulted in the formation of a 200 nm shell

diameter, resulting in an array of laterally-spaced core-shell vertical NWs.[35] For the thicker AlAs shell sample, a significantly thicker AlAs shell layer of ~2 μm was grown during 15 h, causing coalescence of the neighboring vertical NWs, and resulting in the formation of a film-like layer with buried GaAs/AlAs structures. Further details on the sample preparation are provided in Methods.

Figure 1 (a) show a photo of the Si wafer surface covered with the thinner AlAs shell sample of NWs array, as shown in the scanning electron microscopy (SEM) image in Fig. 1 (b). The cross-sectional SEM imaging of this sample in Fig. 1 (c), shows the array of individually-spaced NWs with a ~130 nm core diameter and a thin AlAs shell grown during 1.5 hours. An outermost GaAs layer was grown on the NWs to mitigate the natural oxidation and easy deformation of the AlAs shell layer due to its unstable nature when exposed to air.[49-51] The GaAs outermost shell can prevent drastic oxidization without deteriorating the crystal structure and cracking of the AlAs shell, as shown in the supporting information.[52] The top-view SEM image in Fig. 2(b) shows no surface cracks within the NWs in contrast to the GaAs/AlAs core-shell nanowires without GaAs outermost layer shown in Fig. S1 (e-g) (Supporting information). The outermost GaAs layer thus efficiently suppresses the deformation and cracking of the nanowires.

Figure 1(d) shows a cross-sectional bright-field scanning transmission electron microscopy (BF-STEM) image of a few NWs demonstrating their lateral spacing and vertical core-shell geometry. Figures 1 (e) and (f) show the high-angle annular dark field (HAADF)-STEM image and energy dispersive x-ray spectroscopy (EDS) mapping of the tip, and the HAADF image and EDS mapping of the NW midsection, respectively. The elemental distribution maps indicate that oxidation occasionally progresses from the area with the small Ga distribution on the outermost surface. In addition, the distribution of As is reduced in areas with abundant O, confirming that As is replaced by O due to the natural oxidation of AlAs.

Figures 2 (a) shows an image of the Si wafer covered with the NWs array sample with thicker (2 μm) AlAs shell diameter obtained during 15-h growth time, as shown in the SEM image in Fig. 2 (b). These observations were recorded within two days following the sample' growth. Similarly to the thinner AlAs shell sample, a GaAs layer was grown during the last stage of the entire structure fabrication to preserve the sample from the drastic oxidation, as described above. The top-view SEM image in Fig. 2 (b) shows the NWs coalesced with neighboring wires forming a film-like layer with a buried GaAs/AlAs structure (as illustrated in Fig. 2 (c)), reflecting the morphology of the individual wire tips, which can be recognized by the hexagonal aggregation. No cracks were observed on the sample surface at this stage.

However, the sample structure showed significant changes after being exposed to ambient air for two weeks. Figure 2 (d) shows an image of the Si wafer at this stage, wherein a wide central area appears dark. The surrounding bright area around the edge of the wafer was observed in SEM, showing the initial coalesced NWs array with clearly visible cracks on the surface, as shown in Fig. 2 (e). The corresponding cross-sectional SEM image in Fig. 2 (f) highlights the thick upper part of the coalesced NWs and their thin root parts with voids and cracks, creating spacing between the wires on their lower end. Figure 2 (g) shows an optical microscope image of the boundary between the bright and dark regions as delimited in Fig. 2 (d). Surface layers appear peeled off throughout the dark area in the image. Figure 2 (h) shows SEM images of the rolled-up cylindrical structures identified by white arrows in Fig. 2 (g). As clearly shown in Figure 2(e), even with the presence of a GaAs protective layer, the occurrence of cracks on the surface of the NWs did not result in either delamination or the formation of a cylindrical shape. The rolled-up structure can only be obtained when the GaAs protective layer on the surface effectively prevents cracking. By contrast to the structure of the surface in the bright area of the Si wafer, the imaging of the dark area reveals thin and small-diameter nanowires remaining from the broken lower ends of the original lengthy and

thick wires shown in Fig. 2 (f). Some remaining core GaAs NWs are still identified in this area, as seen in the inset of Fig. 2(i). This result is also confirmed by the cross-sectional SEM in Fig. 2(j), wherein the root part of the wire is broken, and the thick upper part that coalesces with the adjacent wire has disappeared.

Figure 3(a) shows the schematic illustrations of the structural deformations mechanism of nanowires based on the results obtained thus far. For the as-grown sample, the AlAs shell diameter expands and coalesces at the top of the wire, as shown in Fig. 2. Meanwhile, the NWs roots are strongly affected by the shadowing effect that shields the impinging of the beam during the molecular beam epitaxial growth. Consequently, the shell growth at the root is partially inhibited and becomes thinner. This results in a structure similar to Fig. 2(f), with voids at the NW roots.[46] Natural oxidation progresses through the structure by leaving the sample exposed to ambient air for several weeks, thereby forming an oxidized AlAs layer, AlO_x.[38] At this stage, the lattice constant of the crystal substituted with O, with an atomic radius of 0.48 Å smaller than that of As having 1.14 Å, decreases, inducing local deformation due to large tensile strains.[53] The upper side of the sample forms a membrane through the coalescence of NWs tops, which results in shrinking the structure as indicated by the green arrows in the bottom left of Fig 3 (a), and consequently breaking the thin part of the wires at the root base. Consequently, the upper membrane rolls up on the surface (Fig. 3(a)), as reported for thin films[1,2], leaving only the thin root portion of the NWs on the wafer's surface.[7]

A part of the peeled membrane in a rolled-up cylinder was investigated using SEM-EDS, as shown in Figs. 3 (b–g). On the nanowire sample surface at the top of the image, a Ga signal originating from the GaAs protective layer is observed, as shown in Fig. 3(c). As signals are observed throughout in Fig. 3(d), suggesting that a GaAs layer remains inside. In a region different from the Ga signal observed in Fig.3(c), the Al and O signal intensities are strong, as shown in Figs. 3 (e,f), indicating that AlO is formed below the surface. Figure 3 (g) shows the

EDS maps resulting from superimposing the Ga, O, and As signals, which confirm the validity of the suggested mechanism discussed in Fig. 3 (a).

Figure 4 shows an SEM image of a typical rolled-up cylinder membrane transferred to another Si substrate from the initial substrate where the growth was carried out (See, S1 in the supporting information). We obtained a cylinder with a diameter of 300 μm and a thickness of 12 μm. According to Prinz's empirical formula, the diameter D is obtained by $D=d/\varepsilon$, where d is the thickness and ε is the lattice mismatch. It is then considered that the lattice mismatch, which was almost negligible in the GaAs/AsAs system after crystal growth, has been generated by natural oxidation to about 0.04. The cylinder density obtained in this study was 29 cm^{-2}, yielding about 320 cylinders from the delaminated area of the 2-inch silicon substrate.

Transfer can be easily performed by simply shaking off the surface membranes of the sample, and its enlarged images of the inner and outer surfaces is shown in Figs. 4 (b) and (c), respectively. The thin, independent nanowires are observed on the outer surface, whereas wires with a larger diameter are observed on the inner surface. These results align with the formation mechanism described in Fig. 3 (a).

Figure 5(a) shows a schematic diagram of the cylinder and the measurement dimensions; To confirm emission from within the structure, spatially resolved CL measurements were conducted on fragments of the cylinder, where it had been split to expose the internal surface. Further details are provided in Supplementary Information S4. Figs. 5 (b)-(k) were investigated from the inner side. Figure 5(b) is an SEM image of the outer surface of a cylinder sample for the spotted CL measurement, with an enlarged area shown in Fig. 5(c). Fig. 5(d) shows the series of CL spectra at the positions numbered in (c), measured at an acceleration voltage (V_{ac}) of 30 kV. Changing the accelerating voltage for CL measurements

varies the penetration depth of the injected electrons.[54] When considering the penetration of electron beams into GaAs, the penetration depth is estimated to be about 100 nm , 1.5 μm and deeper than 3 μm at 3 kV, 15 kV, and 30kV, respectively.[55,56] In spots #1, #6, and #7 at NW tips, where the GaAs core is covered by partially oxidized thick AlAs shell, a broad band emission was observed in the visible region originating from AlAs at 2.1 eV[57] and AlO_x at 2.7 eV and 3.4 eV, [46,47] in addition to the 1.40 eV peak corresponding to the GaAs band edge emission.[58] In spots #2, #4, #8, #9, and #3, #5, #10 at the deeper positions where the electron beam irradiates the AlO_x shell, visible band emission originating from the AlO_x were dominantly observed. The surface GaAs layer prevents the internal GaAs core and thick AlAs shell of samples #1, #6, and #7 from oxidation, allowing them to show the luminescence from GaAs band edge. The peak observed at an accelerating voltage of 30 kV suggests that not only the outermost GaAs surface but also the inner GaAs core maintains its luminescent characteristics. In contrast, in spots #3, #5, and #10 where the nanowire (NW) is thin and exposed to the surface, thin AlAs shell surrounding GaAs core undergo full oxidation, leading to dominant non-radiative recombination at GaAs core / AlO_x shell interfaces. Consequently, GaAs light emission is suppressed.[46] Figures (e-f) show monochromatic CL images of the corresponding area in (b) at V_{ac} of 30 kV, using the indicated CL detection energies of (e) 3.4 eV, (f) 2.7 eV, (g) 2.1 eV, and (h) 1.4 eV, which support the discussion of the luminescent properties mentioned above. We can observe the luminescence of the GaAs tip and surrounding AlO_x shells investigated from the outer side of the rolled-up cylinder. Figure 5 (i) shows an SEM image of the other area of the inner surface of a rolled-up cylinder for the spotted CL measurement and (j) the series of CL spectra on the spots at the positions numbered in (i) measured at the V_{ac} of 15 kV. In spots #1 to #3, where thick AlAs shell surrounding GaAs core is partially oxidized near the surface, a broad emission band in the visible region with peaks at 2.11, 2.76, and 3.4 eV in addition to the 1.40 eV peak were as in Fig. 5 (c). The vertical lines in the CL spectra in Fig. 5 (k) are guides for the eye for the

observed peaks. In spots #4 to #6, where thick AlAs shell surrounding GaAs core remain unoxidized near the surface, a peak of 1.40 eV originating from the GaAs band edge was dominantly observed. In addition, weak light emission of the visible band was observed in spots #7 to #9 where the electron beam was irradiated to void positions and back-scattered electrons mainly excite the oxide shell regions.

Figure 5 (k) shows CL spectra at spot #2 measured at different acceleration voltages of 3 kV and 15 kV. The overall shape of the CL spectrum and the intensity ratio of each emission peak do not change significantly concerning the accelerating voltage between 3 kV and 15 kV. As shown in Figs. 5(b-c), GaAs NWs approximately 8 μm in length are embedded within the sample. These findings suggest that the GaAs NWs inside the sample retain their light-emitting properties. These spatial dependencies of the CL emission indicate that the cylinder is composed of a GaAs core and the AlO_x shell, and that the GaAs core retains reliable luminescent performance after being rolled-up to form a cylinder.

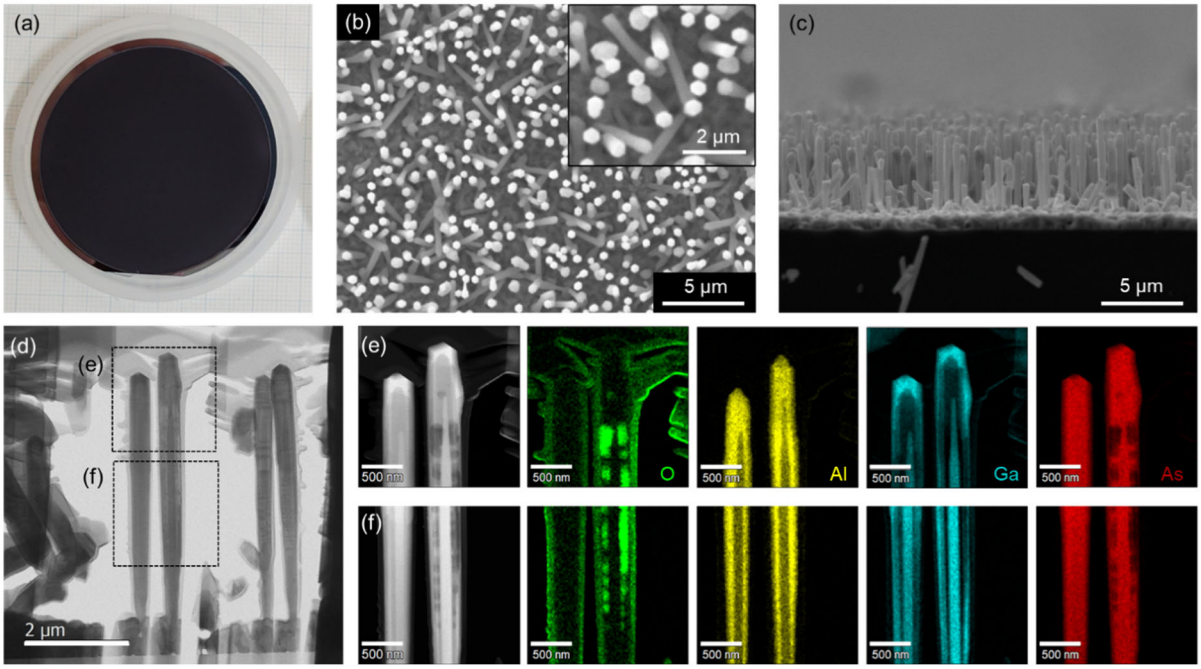

Figure 1. (a) Photo of 2" Si wafer after the growth of the NWs array sample, (b) planar SEM and (c) cross-sectional SEM images of laterally-spaced vertical NWs in the sample with 1.5-h shell growth time and outermost GaAs layer without a buried structure. (d) BE-STEM image and (e,f) HAADF-STEM, energy dispersive x-ray spectroscopy measurements for O, Al, Ga, and As with shell growth time of 1.5-h with the outermost GaAs shell.

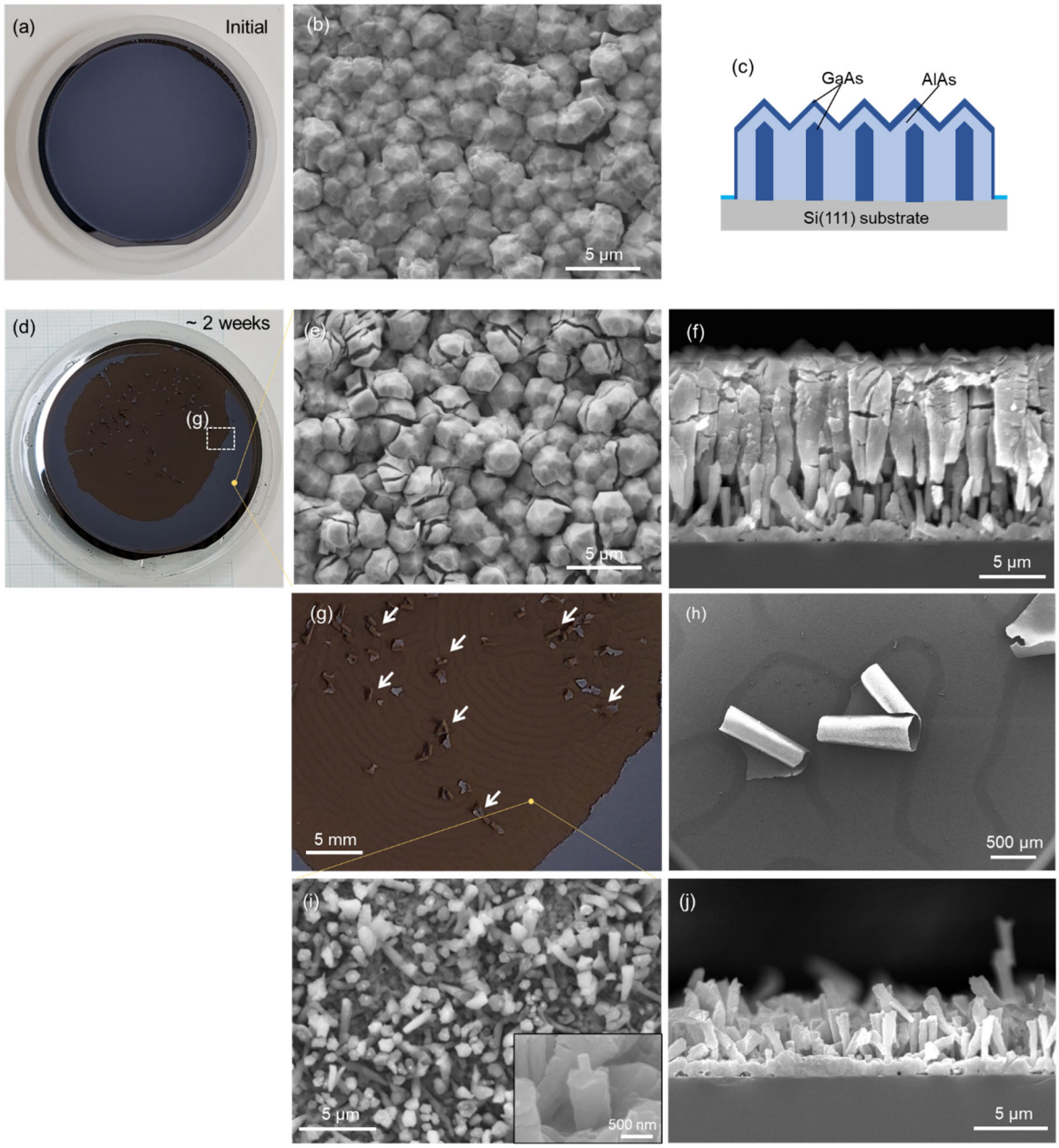

Figure 2. (a,b) Appearance of the coalesced NW sample with a thick AlAs shell layer grown for 15 hours; sample of the Si wafer surface after the growth within two days, (a) the appearance, (b) plan-view SEM, and (c) schematically illustrated nominal cross-sectional structure of the sample. (d–j) Observation of the coalesced NWs sample after two weeks of exposition to ambient air, where the surface membrane was peeled off. (d) Photo of the Si wafer at this stage; (e) enlarged SEM image of the bright area near the edge of the wafer; and (f) their cross-sectional SEM image. (g) optical microscope surface observations as delimited in (d) at the border area with remaining NWs, wherein the upper part of the wires were peeled off at the areas indicated by the white arrows; (h) and SEM surface observation of the enrolled membrane, plan-view surface SEM image (g) at the area preserving the coalesced NWs, and (h) the area after the top part was peeled off, where the inset shows enlarged tilted image of the broken NWs, and (i) cross-sectional SEM image of the broken NWs at the root end.

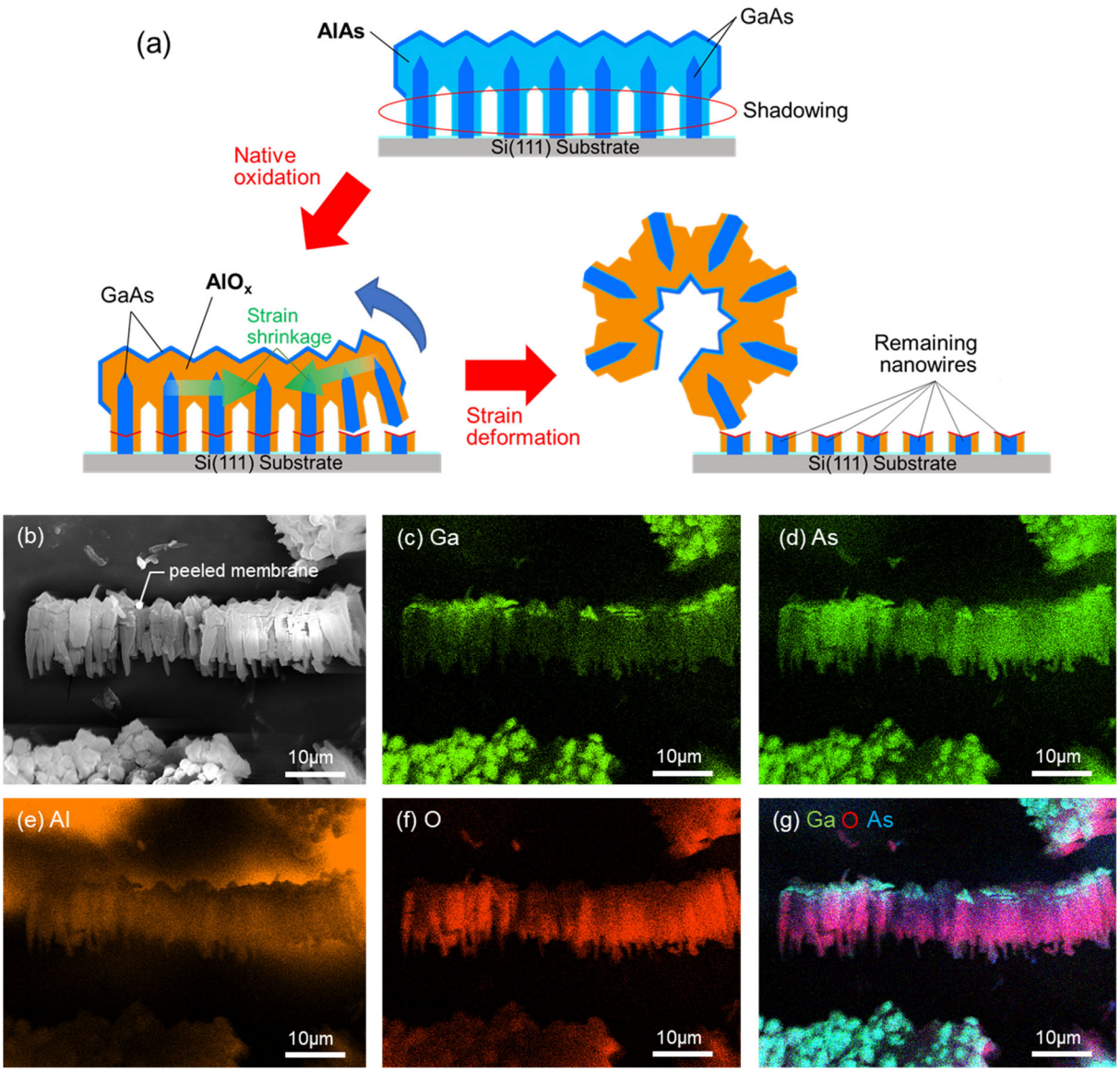

Figure 3. (a) Schematic diagram of cylinder formation mechanism in buried GaAs/AlAs core-shell nanowires. Cross-sectional (b) SEM observation, and corresponding EDS elemental mapping for (c) Ga, (d) As, (e) Al, (f) O, and (g) superimposed mapping of Ga, O, and As for the peeled off membrane.

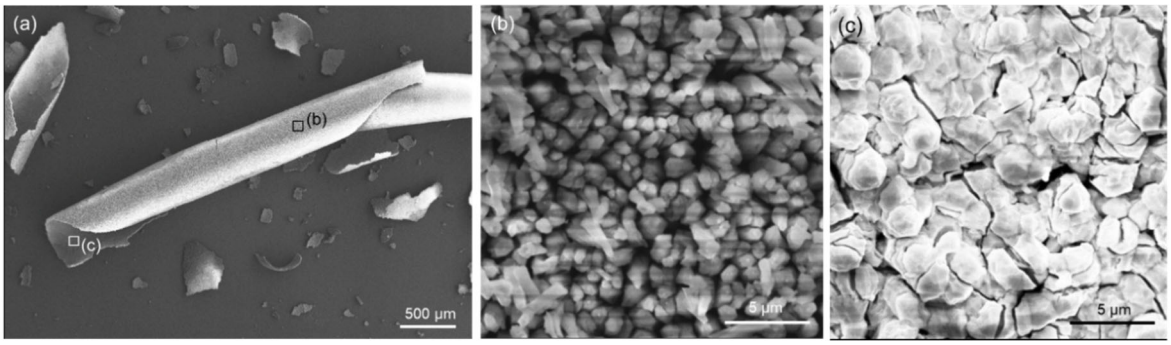

Figure 4. (a) SEM observation of a typical cylinder transferred to another silicon substrate and enlarged images of (b) inner and (c) outer surfaces, respectively.

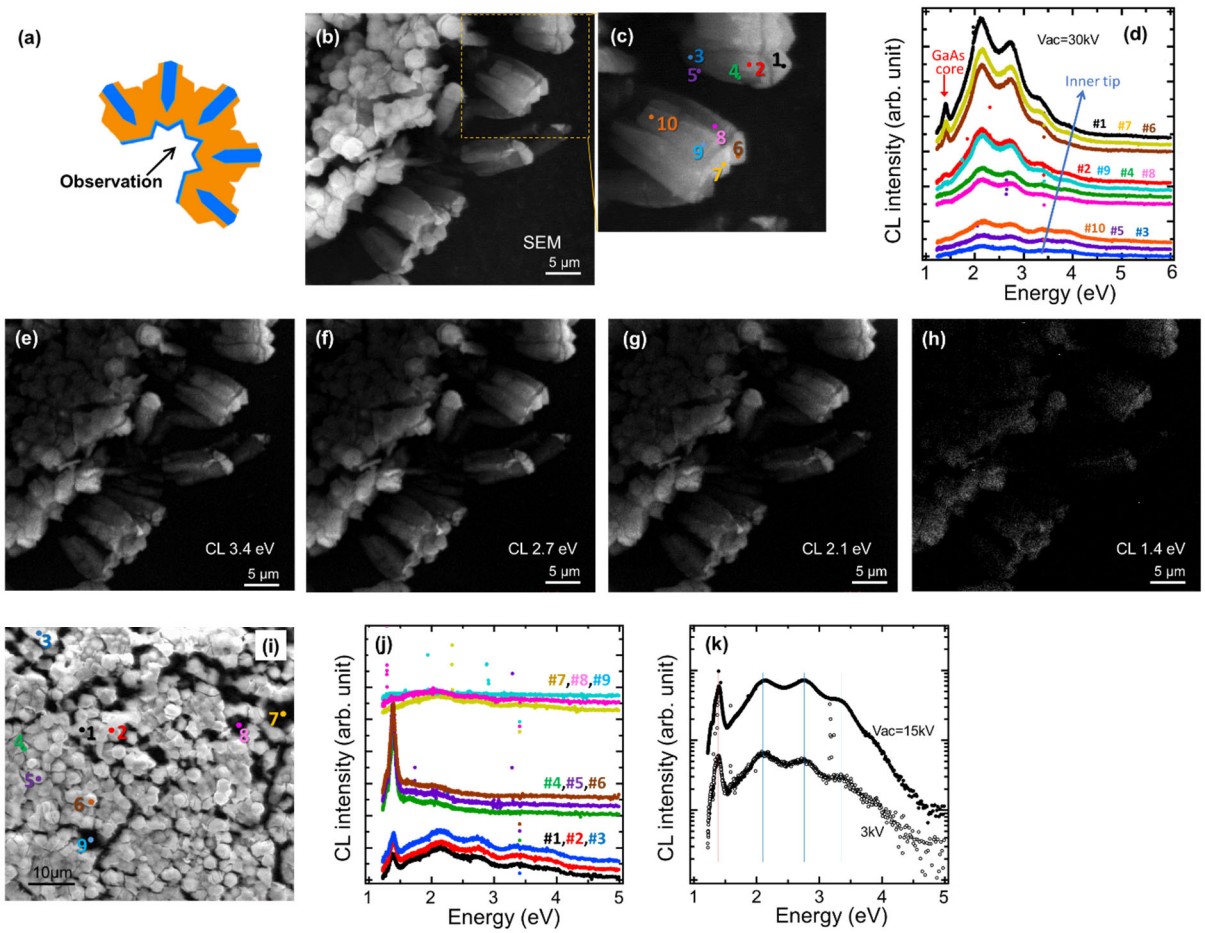

Figure 5. (a) Schematic diagram of a rolled-up cylinder and the measurement dimensions; (b)-(h) were investigated from the outer side and (i)-(k) from the inner side. (b) SEM image of the outer surface of a cylinder sample for the spotted CL measurement with the enlarged area shown in (c), and (d) the series of CL spectra at the positions numbered in (c), measured at a V_{ac} of 30 kV. (e-h) Monochromatic CL images of the corresponding area in (b) at a V_{ac} of 30 kV, using the indicated CL detection energies of (e) 3.4 eV, (f) 2.7 eV, (g) 2.1 eV, and (h) 1.4 eV. (i) SEM image of the other area of the inner surface of the cylinder sample for the spotted CL measurement and (j) the series of CL spectra on the spots at the positions numbered in (i) measured at the acceleration voltage 15 kV. (k) CL spectra at spot #2 measured at different acceleration voltages of 3 and 15 kV. The vertical lines in the CL spectra of (k) are guides for observable peaks at 1.40 eV originates from GaAs, 2.11 eV from AlAs, and 2.76 and 3.4 eV from AlO_x. [46,47,57]

3. Conclusion

In summary, we demonstrated the fabrication of rolled-up cylindrical membranes composed of GaAs nanowires embedded in AlO_x medium, through the strain deformation of buried GaAs/AlAs core-shell nanowires by natural oxidation. The NWs array sample formed a film-like membrane with a buried structure by growing a thick AlAs shell leading to the coalescence of adjacent NWs in the array. The sample surface on Si wafer peeled off after a prolongated exposure to ambient air, leading to the formation of characteristic cylindrical structures consisting of enrolled GaAs/AlO_x core-shell nanowires, typically having 300 μm diameter and a few mm length. The GaAs outermost layer grown on top of the NWs array contributed to minimizing the rapid oxidation and crack generation, and acts as a surface protective layer with little deterioration, enabling the eventual formation of rolled-up cylindrical structures. Etching of a sacrificial layer was unnecessary, as the nanowires spontaneously fracture near their bases due to strain-induced forces. This process led to the self-formation of a microtube that encapsulates the NWs. The membrane can be easily transferred by simply shaking off the surface membranes of the sample. The obtained cylinders showed preserved optical properties associated with the GaAs nanowire's core within the structure surrounded by the native oxides. Our findings suggest the utilization of ensembles of nanoscale optical materials within controlled geometrical structure with area-saving and transferable features.

4. Methods

The GaAs/AlAs core-shell nanowire (NW) sample on Si(111) substrates was prepared by self-catalyzed molecular beam epitaxy (MBE). [38,46] The substrate surface had not been treated prior to growth and was covered with a typical native oxide layer of a few nm in thickness. [22] The Ga supply rate was set to match a planar growth rate of 1.0 ML/s, and the Al supply rate to match 0.52 ML/s on GaAs(001). The corresponding beam equivalent pressures are 8.0×10^{-5} Pa for Ga and 1.8×10^{-5} Pa for Al, respectively. The GaAs core growth was initiated by opening

the Ga shutter under As_4 overpressure at 6×10^{-4} Pa, where the GaAs core was grown for 30 min at 560℃. [59] Then, we obtained the nanowires having GaAs core with their length about 5 μm and the diameter about 130 nm. Next, the growth was interrupted for 15 min to crystalize the Ga catalyst, and the As_4 pressure was increased to 1.0×10^{-3} Pa. Subsequently, the lateral growth became dominant, generating core-shell NWs.[46] Then, the GaAs shell layer was grown for 10 min, and subsequently, AlAs was grown to form the GaAs/AlAs heterostructures shell structure.[46] The width of the AlAs was controlled by the growth time of the layer for 1.5 and 15 h, forming individually spaced nanowires, and coalesced nanowires to form a buried entire structure, respectively. Nominally, a ~50-nm GaAs layer was grown for 15 min at the outermost surface as a preservation layer to prevent drastically rapid oxidation of the AlAs.

After the nanowires' growth, the samples were left exposed to ambient atmosphere to form native oxides AlOx transferred from the AlAs.[38,39] The Al-rich AlGaAs shell selectively underwent native oxidation as its oxidation rate differed significantly from that of the GaAs core.[39] The rolled-up structure was formed by exposing the samples to typical climatic conditions of the southwestern region of Japan, where the experiment was conducted. The temperature and humidity ranged from 5°C to 15°C and 40% to 70%, respectively, which may have influenced the oxidation rate and resulting properties.[60-62] The rolled-up structure was obtained through natural oxidation in this environment, where the oxidation progressed slowly. We investigated the structural characteristics of the NWs using scanning electron microscopy (SEM, JSM-7610F, JEOL, Japan) with energy dispersive Xray spectroscopy (EDS). We also performed cross-sectional scanning transmission electron microscopy (STEM, JEM-ARM200F, JEOL, Japan) operating at 200 kV, equipped with an energy dispersive X-ray (EDX) spectroscopy imaging system (JED-2300T, JEOL, Japan). For transmission electron microscopy (TEM) measurements, finely sliced samples displaying thicknesses under 200 nm were fabricated using a focused ion beam system (FEI Strata DB 235). To investigate the optical characteristics of NWs at room temperature, combined SEM/cathodoluminescence (FE-SEM,

S-4300, Hitachi High-Tech, Japan / CL, MP-32M, Horiba, Japan) investigations were conducted to identify the local characteristics of the NW luminescence. [58,63,64] All measurements were performed at room temperature.

Supporting Information

Supporting Information is available from the Wiley Online Library or from the author.

Acknowledgements

This study was partly supported by the funding support from KAKENHI (Nos. 23H00250, 21KK0068, 19H00855, 16H05970) from Japan Society of Promotion of Science.

Received: ((will be filled in by the editorial staff))

Revised: ((will be filled in by the editorial staff))

Published online: ((will be filled in by the editorial staff))

References

[1] S. Vicknesh, F. Li, Z. Mi, *Appl. Phys. Lett.* **2009**, *94* (8), 081101.

[2] R. Songmuang, C. Deneke, O. G. Schmidt, *Appl. Phys. Lett.* **2006**, *89* (22), 223109.

[3] V. Ya. Prinz, V. A. Seleznev, A. K. Gutakovsky, A. V. Chehovskiy, V. V. Preobrazhenskii, M. A. Putyato, T. A. Gavrilova, *Physica E*. **2000**, *6* (1–4), 828–831.

[4] O. G. Schmidt, K. Eberl, Nature (London). **2001**, 410, 168.

[5] M. Hosoda, Y. Kishimoto, M. Sato, S. Nashima, K. Kubota, S. Saravanan, P. O. Vaccaro, T. Aida, N. Ohtani, *Appl. Phys. Lett*. **2003**, *83* (5), 1017–1019.

[6] P. Song, C. Chen, J. Qu, P. Ou, M. H. T. Dastjerdi, Z. Mi, J. Song, X. Liu, *Nanotechnology*. **2018,** *29* (41), 415501.

[7] F. Li, Z. Mi, *Opt. Express*. **2009**, *17* (22), 19933–19939.

[8] A. Khandelwal, Z. Ren, S. Namiki, Z. Yang, N. Choudhary, C. Li, P. Wang, Z. Mi, X. Li, *ACS Appl. Mater. Interfaces* **2022**, 14, 25.

[9] Z. Yang, M. D. Kraman Z. Zheng, H. Zhao, J. Zhang, S. Gong, Y. V. Shao, W. Huang, P. Wang X. Li *Adv. Func. Mater.* 2020, 30, 2004034.

[10] W. Huang, X. Yu, P. Froeter, R. Xu, P. Ferreira, X. Li *Nano Lett.* **2012**, 12, 12, 6283–6288.

[11] M. Djavid, X. Liu, Z. Mi, *Optics Express.* **2014**, Vol. 22, Issue S7, pp. A1680-A1686.

[12] I. S. Chun, A. Challa, B. Derickson, K. J. Hsia, X. Li, *Nano Lett.* **2010**, 10, 10, 3927–3932.

[13] M. Müller, F. Bertram, P. Veit, B. Loitsch, J. Winnerl, S. Matich, J. J. Finley, G. Koblmüller, J. Christen, *Appl. Phys. Lett.* **2019**, *115* (24), 243102.

[14] F. Qian, S. Gradečak, Y. Li, C. Y. Wen, C. M. Lieber, *Nano Lett.* **2005**, *5* (11), 2287–2291.

[15] K. Tomioka, J. Motohisa, S. Hara, Hiruma, K. Fukui, T. *Nano Lett*. **2010**, *10* (5), 1639–1644.

[16] B. Mayer, D. Rudolph, J. Schnell, S. Morkötter, J. Winnerl, J. Treu, K. Müller, G. Bracher, G. Abstreiter, G. Koblmüller, J. J. Finley, *Nat. Commun.* **2013**, *4*, 2931.

[17] D. Saxena, S. Mokkapati, P. Parkinson, N. Jiang, Q. Gao, H. H. Tan, C. Jagadish, *Nat. Photonics.* **2013**, *7* (12), 963–968.

[18] T. Bryllert, L.-E. Wernersson, L. E. Froberg, L. Samuelson, *IEEE Electron Dev. Lett*. **2006**, *27* (5), 323–325.

[19] K. Tomioka, M. Yoshimura, T. Fukui, *Nature*. **2012**, *488* (7410), 189–192.

[20] J. Wallentin, N. Anttu, D. Asoli, M. Huffman, I. Åberg, M. H. Magnusson, G. Siefer, P. Fuss-Kailuweit, F. Dimroth, B. Witzigmann, H. Q. Xu, L. Samuelson, K. Deppert, M. T. Borgström, *Science*. **2013**, *339* (6123), 1057–1060.

[21] E. Garnett, L. Mai, P. Yang, *Chem. Rev*. **2019**, *119* (15), 8955–8957.

[22] T. Tanigawa, R. Tsutsumi, F. Ishikawa, *Jpn. J. Appl. Phys*. **2022**, *61* (SD), SD1005.

[23] J. Hu, T. W. Odom, C. M. Lieber, *Acc. Chem. Res*. **1999**, *32* (5), 435–445.

[24] C. M. Lieber, *MRS Bull*. **2003**, *28* (7), 486–491.

[25] L. Samuelson, *Mater. Today*. **2003**, *6* (10), 22–31.

[26] Z. L. Wang, *Mater. Today*. **2004**, *7* (6), 26–33.

[27] P. Yang, *MRS Bull*. **2005**, *30* (2), 85–91.

[28] X. Duan, Y. Huang, Y. Cui, J. Wang, C. M. Lieber, *Nature*. **2001**, *409* (6816), 66–69.

[29] Z. Zhong, F. Qian, D. Wang, C. M. Lieber, *Nano Lett*. **2003**, *3* (3), 343–346.

[30] H. Kim, Y. Cho, H. Lee, S. I. Kim, S. R. Ryu, D. Y. Kim, T. W. Kang, K. S. Chung, *Nano Lett*. **2004**, *4* (6), 1059–1062.

[31] F. Qian, Y. Li, S. Gradečak, D. Wang, C. J. Barrelet, C. M. Lieber, *Nano Lett.* **2004**, *4* (10), 1975–1979.

[32] Y. Huang, X. Duan, C. M. Lieber, *Small.* **2005**, *1* (1), 142–147.

[33] M. H. Huang, S. Mao, H. Feick, H. Yan, Y. Wu, H. Kind, E. Weber, R. Russo, P. Yang, *Science*. **2001**, *292* (5523), 1897–1899.

[34] J. C. Johnson, H. J. Choi, K. P. Knutsen, R. D. Schaller, P. Yang, R. J. Saykally, *Nat. Mater*. **2002**, *1* (2), 106–110.

[35] X. Duan, Y. Huang, R. Agarwal, C. M. Lieber, *Nature*. **2003**, *421* (6920), 241–245.

[36] R. Agarwal, C. J. Barrelet, C. M. Lieber, *Nano Lett*. **2005**, *5* (5), 917–920.

[37] J. M. Dallesasse, N. Holonyak, *J. Appl. Phys*. **2013**, *113* (5), 051101.

[38] R. Tsutsumi, N. Tsuda, B. Zhang, W. M. Chen, I. A. Buyanova, F. Ishikawa, *Appl. Phys. Express*. **2020**, *13* (7), 075003.

[39] D. L. Huffaker, D. G. Deppe, K. Kumar, T. J. Rogers, *Appl. Phys. Lett.* **1994**, *65* (1), 97–99.

[40] A. R. Sugg, N. Holonyak, Jr., J. E. Baker, F. A. Kish, J. M. Dallesasse, *Appl. Phys. Lett*. **1991**, *58* (11), 1199–1201.

[41] A. R. Sugg, E. I. Chen, N. Holonyak, Jr., K. C. Hsieh, J. E. Baker, N. Finnegan, *J. Appl. Phys*. **1993**, *74* (6), 3880–3885.

[42] E. I. Chen, N. Holonyak, Jr., S. A. Maranowski, *Appl. Phys. Lett.* **1995**, *66* (20), 2688–2690.

[43] K. D. Choquette, K. M. Geib, H. C. Chui, B. E. Hammons, H. Q. Hou, T. J. Drummond, R. Hull, *Appl. Phys. Lett.* **1996**, *69* (10), 1385–1387.

[44] J. M. Dallesasse, N. Holonyak, Jr., *Appl. Phys. Lett.* **1991**, *58* (4), 394–396.

[45] A. Fiore, V. Berger, E. Rosencher, N. Laurent, S. Theilmann, N. Vodjdani, J. Nagle, *Appl. Phys. Lett.* **1996**, *68* (10), 1320–1322.

[46] H. Hibi, M. Yamaguchi, N. Yamamoto, F. Ishikawa, *Nano Lett.* **2014**, *14* (12), 7024–7030.

[47] F. Ishikawa, P. Corfdir, U. Jahn, O. Brandt, *Adv. Opt. Mater*. **2016**, *4* (12), 2017–2020.

[48] K. Minehisa, R. Murakami, H. Hashimoto, K. Nakama, K. Sakaguchi, R. Tsutsumi, T. Tanigawa, M. Yukimune, K. Nagashima, T. Yanagida, S. Sato, S. Hiura, A. Murayama, F. Ishikawa, *Nanoscale Adv*. **2023**, *5* (6), 1651–1663.

[49] W. D. Johnston, Jr., W. M. Callahan, *Appl. Phys. Lett*. **1976**, *28* (3), 150–152.

[50] R. D. Dupuis, P. D. Dapkus, R. D. Yingling, L. A. Moudy, *Appl. Phys. Lett*. **1977,** *31* (3), 201–203.

[51] J. M. Dallesasse, P. Gavrilovic, N. Holonyak, Jr., R. W. Kaliski, D. W. Nam, E. J. Vesely, R. D. Burnham, *Appl. Phys. Lett*. **1990**, *56* (24), 2436–2438.

[52] D. Li, J. Lee, M. Caffrey, *Growth Des*. **2011**, *11* (2), 530–537.

[53] X. Li, *J. Phys. D*. **2008**, *41* (19), 193001.

[54] K. Kanaya, S. Okayama, *J. Phys. D*. **197**2, *5* (1), 43–58.

[55] T. E. Everhart, P. H. Hoff, *J. Appl. Phys*. **1971,** *42* (13), 5837–5846.

[56] H. J. Leamy, *J. Appl. Phys*. **1982,** *53* (6), R51–R80.

[57] H. Kressel, F.H. Nicoll, M. Ettenberg, W. M. Yim, A. G. Sigai, *Solid State Comm.* **1970,** 8(17), 1407-1409.

[58] F. Ishikawa, Y. Akamatsu, K. Watanabe, F. Uesugi, S. Asahina, U. Jahn, S. Shimomura, *Nano Lett*. **2015**, *15*, 7265.

[59] M. Yukimune, R. Fujiwara, H. Ikeda, K. Yano, K. Takada, M. Jansson, W. M. Chen, I. A. Buyanova, F. Ishikawa*, Appl. Phys. Lett*. **2018**, *113*, 011901.

[60] P.O. Vaccaro, K. Koizumi, K. Fujita, T. Ohachi, *Microelectronics Journal*. **1999**, 30, 387–391.

[61] R.V. Ghita, E. Vasile, D. Cengher, *Thin Solid Films.* **1999**, *338*, 46-48.

[62] T. Yoshikawa, H. Saito, H. Kosaka, Y. Sugimoto, K. Kasahara, *Appl. Phys. Lett.* **1998**, *72*(18), 2310–2312.

[63] K. Watanabe, T. Nagata, Y. Wakayama, T. Sekiguchi, R. Erdélyi, J. Volk, *ACS Nano.* **2015** *9*, 2989.

[64] K. Watanabe, T. Nagata, S. Oh, Y. Wakayama, T. Sekiguchi, J. Volk, Y. Nakamura, *Nat. Commun.* **2016**, 7, 10609.

The table of contents entry

Natural oxidation from prolonged ambient exposure drives the delamination of the nanowires array film, forming rolled-up structures. Structural investigation provides an analytical description of this oxidation mechanism. The membranes, maintaining the GaAs core's optical properties, can be transferred by shaking off the surface. The findings suggest potential for compact, transferable semiconductor devices with advanced nanoscale optical functions.

Hidetoshi Hashimoto, Keisuke Minehisa, Kaito Nakama,*

*Kentaro Watanabe, Kazuki Nagashima, Takeshi Yanagida, Fumitaro Ishikawa**

Title *Rolled-up membranes from GaAs/AlOx core-shell nanowire ensembles through natural oxidation*

ToC figure

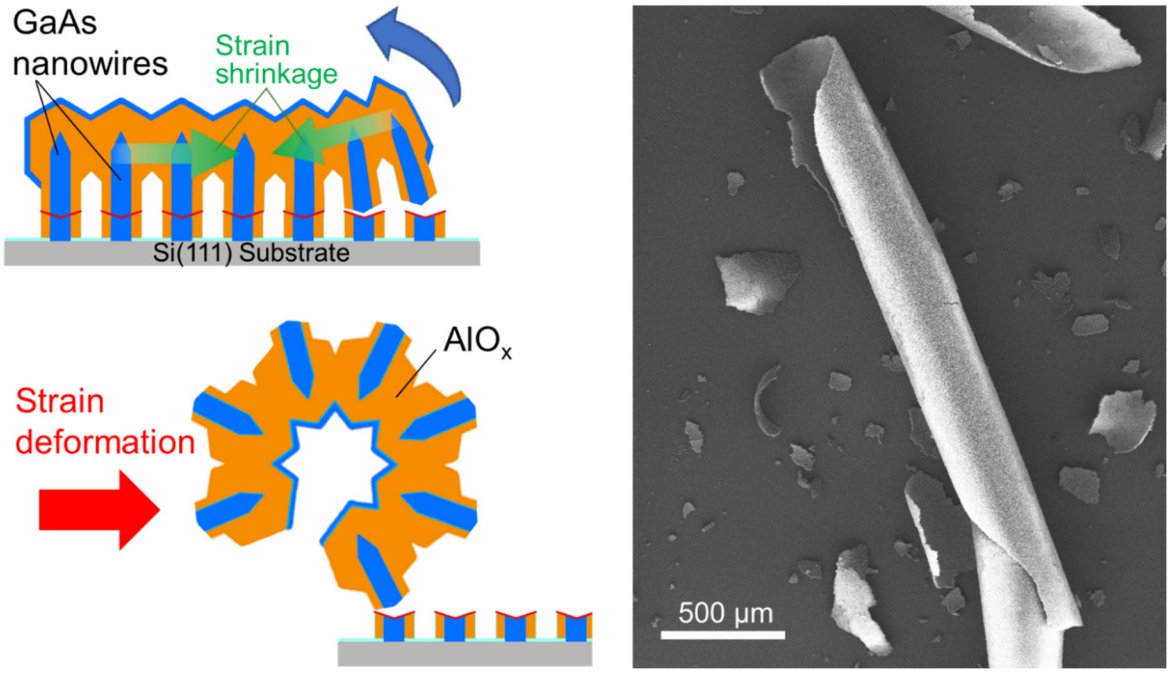

Supporting Information

Title Rolled-up membranes from GaAs/AlOx core-shell nanowire ensembles through natural oxidation

Hidetoshi Hashimoto, Keisuke Minehisa, Kaito Nakama,*
*Kentaro Watanabe, Kazuki Nagashima, Takeshi Yanagida, Fumitaro Ishikawa**

S1. Test samples without the outermost GaAs protection layer

A series of GaAs/AlAs core-shell NWs with variable width of AlAs shells by varying the growth time of the AlAs shell layer were prepared. Figures 1(a)–(c) show the surface observation of the 2-inch Si wafer after the growth and (e–h) show the plan-view SEM images of four different samples. The surface of the first three samples is not covered by the outermost GaAs layers. These samples were grown by varying the growth time of the AlAs shell layer (2, 4, 8 h, those were compared with the sample grown for 15 h described above). We observe the clear formation of NWs, typically with an average GaAs core diameter of approximately 130 nm. The diameter of the NWs increases with the growth time of the AlAs shell layer. Cracks in the nanowires were observed in all samples. These results are attributed to lattice shrinkage due to the natural oxidation of AlAs to AlOx. Notably, high AlAs are chemically unstable in the typical room-temperature atmospheric environment, and "hydrolyzes" into various oxides over time. [39,65,66] The GaAs outermost layer for thin and coalesced NWs shown in Figs. 1–2 in the main text layer suppresses rapid oxidation and crack generation, and by acting as a surface protective layer with little deterioration of itself, it enables the formation of a cylindrical structure.

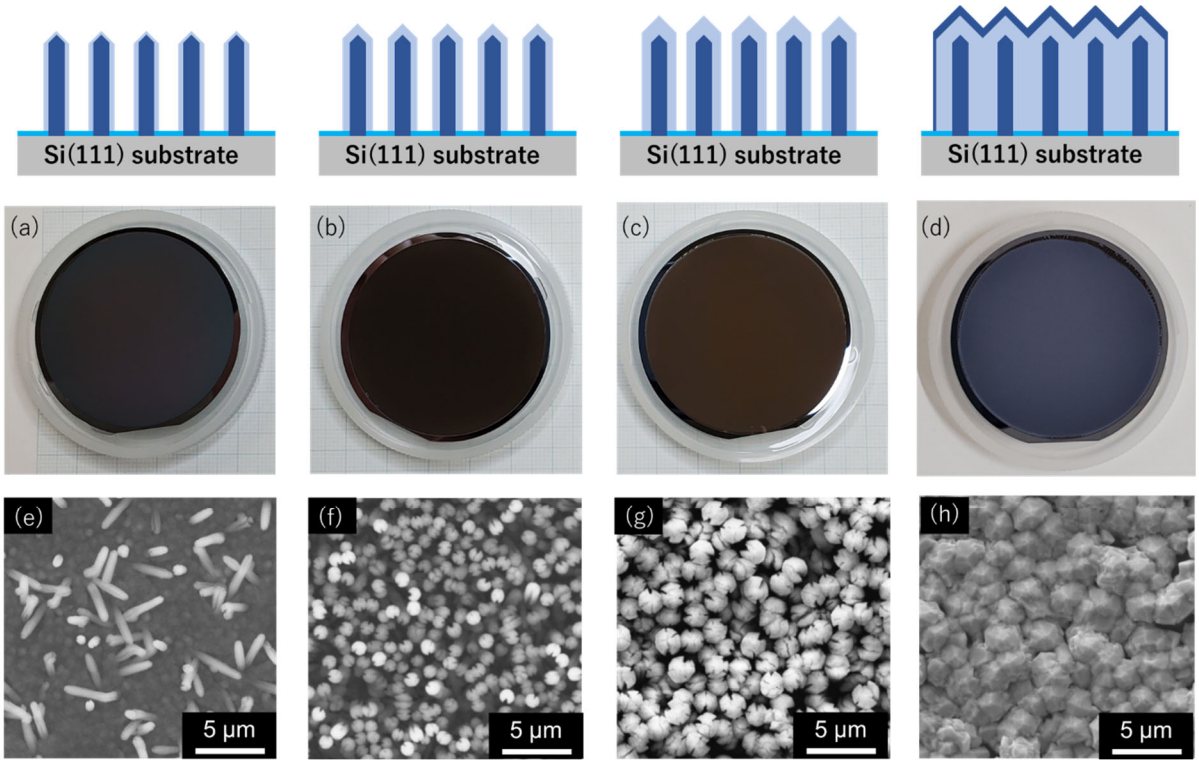

Figure S1. (a–d) The substrate surface and (e–h) SEM observations of the four samples with AlAs shell-growth times of 2, 4, 8, and 15 h, respectively. The last sample are shown in Figs. 2(a) and (c) in the main text.

S2. Example of the other cylinder

Figure S2 shows the appearance and SEM observations of the other typical cylinder transferred to another Si substrate from the initial substrate where the growth was carried out. Transfer can be easily performed by simply shaking off the surface membranes of the sample. The diameter is about 300 μm and comprises numerous enrolled NWs.

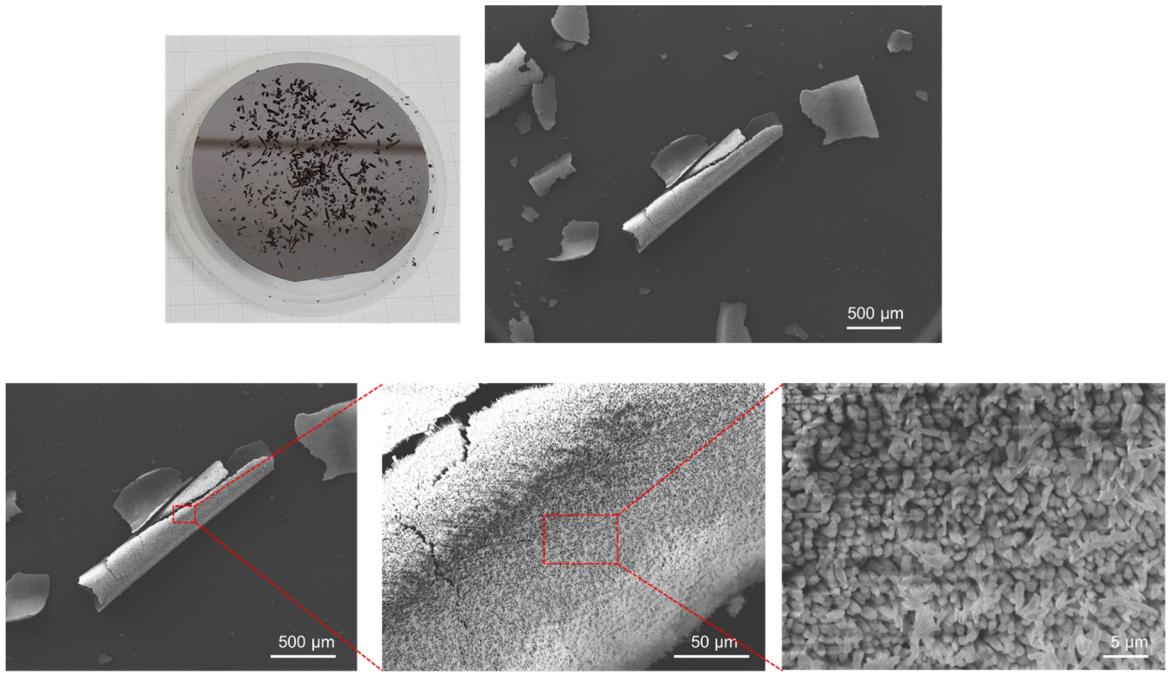

Figure S2. Appearance and SEM observations of the cylinders transferred to the other Si substrate.

Figure S3 show the cross-sectional SEM image (corresponding to Fig. 2(c) of the main text) and the elemental EDS mapping of Ga, As, Al, O, Si, and superimposed image of Ga, O, and As, respectively, as well as the EDS spectrum of a NW sample shown in Figs. 2–5 of the main text obtained from the area preserving the NWs on the Si substrate without peeling off the structure. As seen in the figures, the NWs ensemble coalesces at the upper part of the structure. At the area close to the root, voids emerge from the shadowing effect of the molecular beam during its epitaxial growth where the thinner shell layer was grown compared to the upper part.[46] Part of those areas occasionally breaks due to the strain deformation of the AlAs to AlOx inducing the rolled-up cylindrical structure.

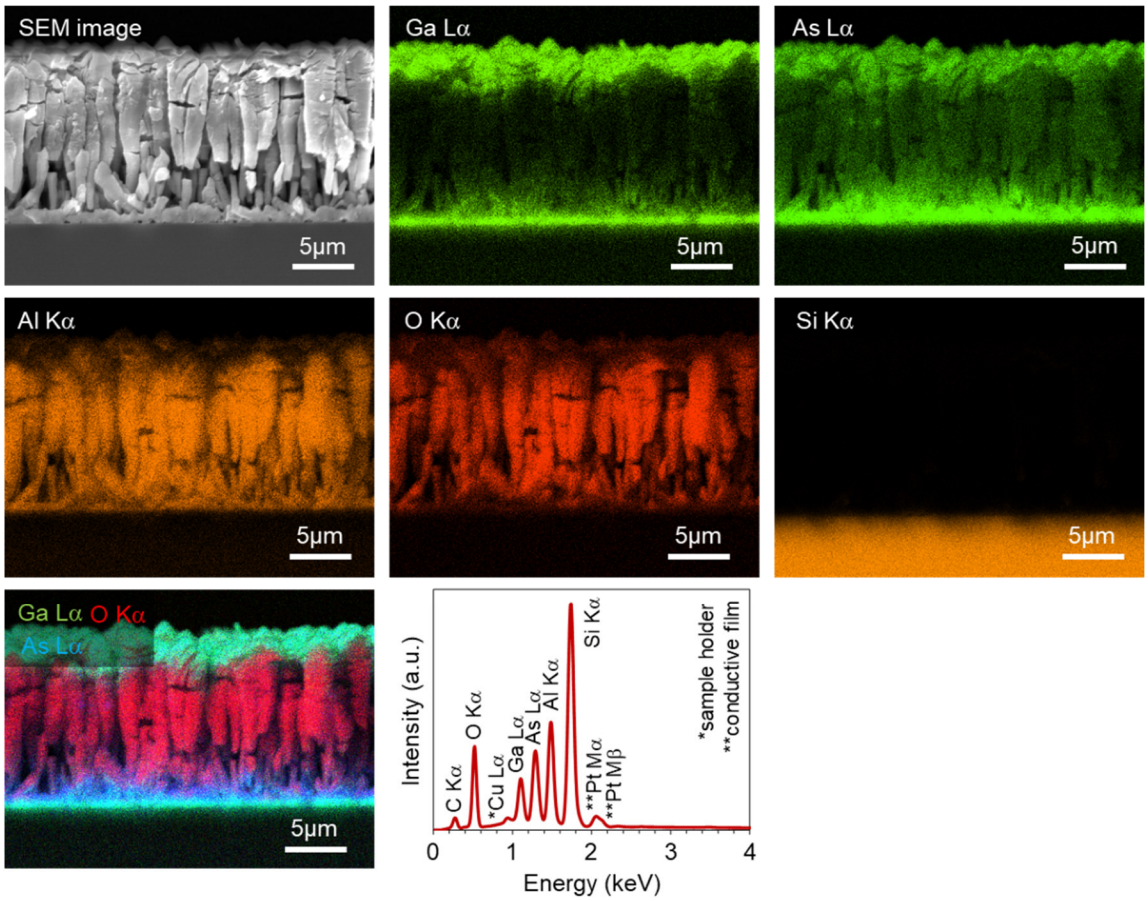

Figure S3. The cross-sectional SEM image (corresponding to Fig. 2(c) of the main text) and the elemental EDS mapping of Ga, As, Al, O, Si, and superimposed image of Ga, O, and As, respectively, and EDS spectrum of a NWs sample shown in Figs. 2–5 of the main text obtained from the area preserving the NWs on the Si substrate without peeling off the upper structure.

Figure S4 shows the cross-sectional SEM image (corresponding to Fig. 2(i) of the main text) and the elemental EDS mapping of Ga, As, Al, O, Si, and superimposed image of Ga, O, and As, respectively, as well as the EDS spectrum of a NW sample shown in Figs. 2–5 of the main text obtained from the area preserving the NWs on the Si substrate after peeling off the upper structure. After the cylinder formation, the area solely preserves the root of the NWs, and no upper parts are observed.

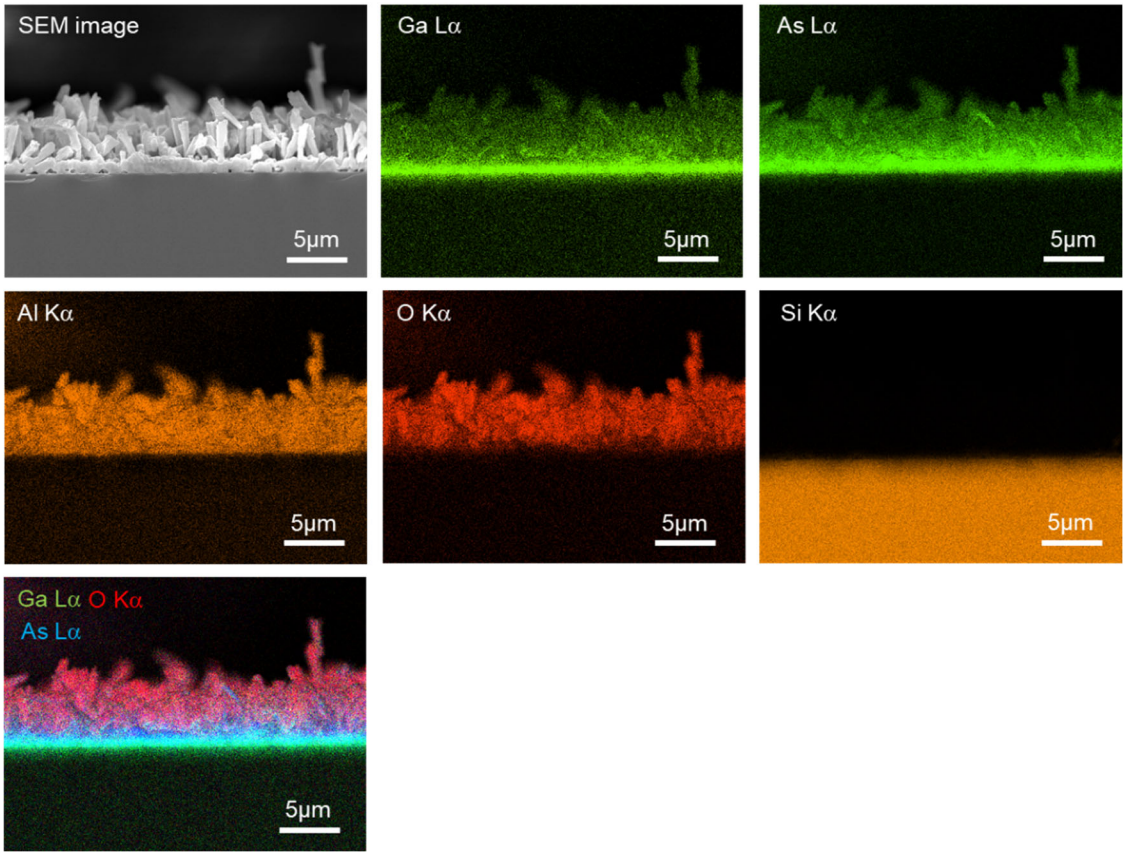

Figure S4. The cross-sectional SEM image (corresponding to Fig. 2(i) of the main text) and the elemental EDS mapping of Ga, As, Al, O, Si, and superimposed image of Ga, O, and As, respectively, as well as the EDS spectrum of a NW sample shown in Figs. 2–5 of the main text obtained from the area preserving the NWs on the Si substrate after peeling off the upper structure.

Figure S5 shows the SEM image of around the border of the area wherein the oxidized upper part of the NWs structure was peeled off or preserved. The area where the wires were preserved shows densely coalesced thick NWs with cracks on their surface.

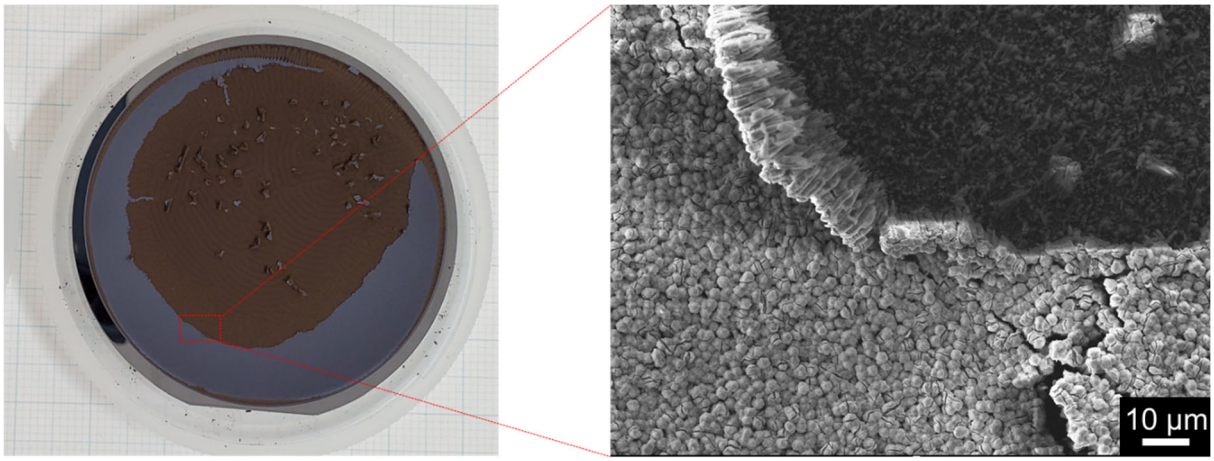

Figure S5. SEM image of the border of the area where the oxidized upper part of the NWs structure was peeled off or preserved.

S3 Photoluminescence

Fig. S6(a) presents the PL measurements for the sample depicted in Fig. 1, along with those for the sample featuring an enlarged AlAs shells (Fig. 2(d)) from the main text, where the rolled-up structure was transferred to a different silicon substrate, corresponding to Supporting Fig. S2 (Fig. S6(b)). Additionally, measurements for the portion of the sample that remained unrolled on the substrate are shown in Fig. S6(c). PL measurements were performed at room temperature (RT) using a micro-PL system. A 532 nm solid-state laser served as the excitation source, and the PL signal was collected in a backscattered geometry through a 20× objective (NA = 0.5) and detected using an InGaAs array coupled to a grating monochromator.

As seen in Fig. S6(a), strong GaAs emission was observed during PL measurements. In contrast, no luminescence was observed from the rolled-up structure (Fig. S6(b)). Very weak luminescence, presumed to be from GaAs, was detected from the portion remaining on the substrate (Fig. 6(c)). Achieving any detectable luminescence required a high excitation intensity (~200 mW) and a long integration time. Furthermore, the luminescence peak exhibited a lower energy of 1.37 eV compared to typical GaAs, suggesting that the sample had been heated to approximately 450 K.[67] The absence of luminescence from the cylindrical structure is consistent with the complexity of the sample and the challenges of effective excitation.

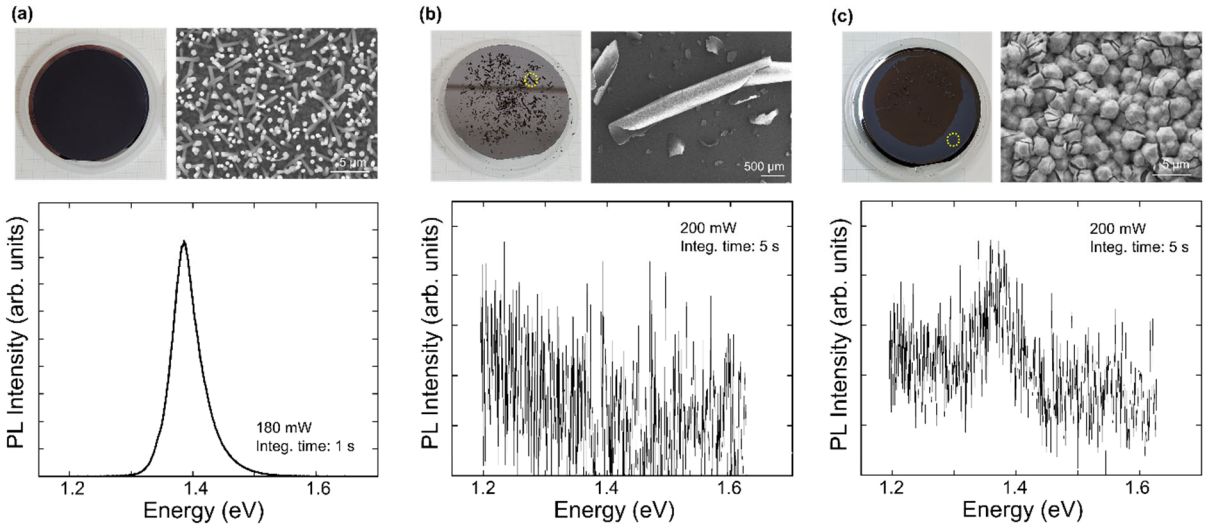

Figure S6. PL measurements (a) for the sample shown in Fig. 1 in the main text, (b) for the sample with enlarged AlAs shells (Fig. 2(d)) where the rolled-up structure was transferred to a different silicon substrate (Supporting Fig. S2), and (c) for the area that remained on the substrate without rolled-up. The yellow dotted circles in the wafer photograph indicate the positions where PL measurements were performed.

S4 Sample preparation for cathodoluminescence measurements

To confirm the emission inside the structure, we divided the cylinder and performed spatially resolved CL measurements on the fragments whose insides were exposed to the surface. The fragments were selected as depicted in Figure S7, with consideration given to their placement on the sample stage, the measurement positions, and the acceleration voltage.

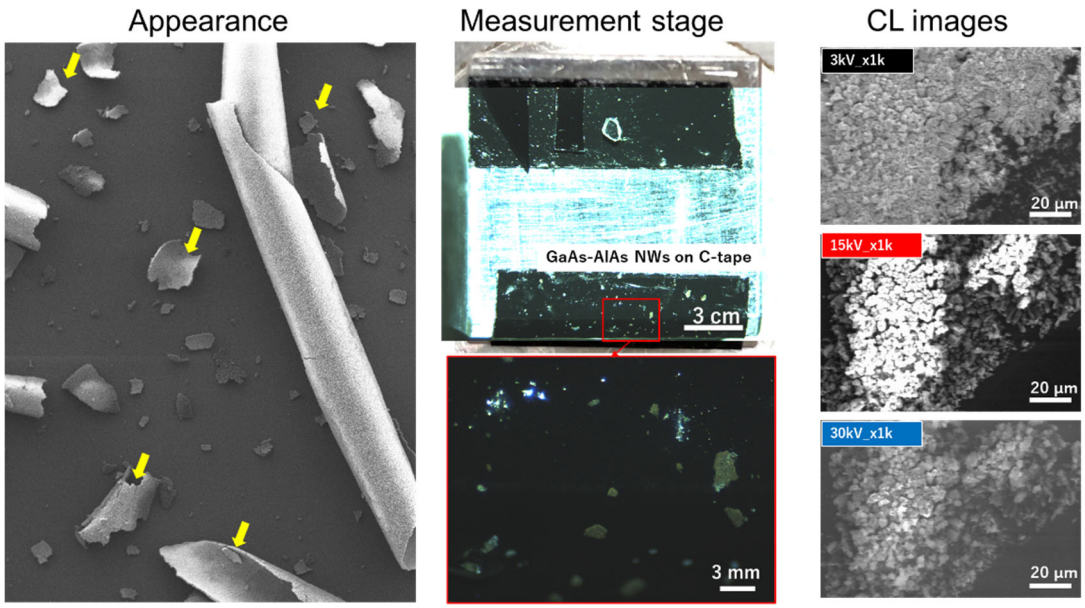

Figure S7. Sample preparation for CL measurements: Appearance of the sample fragment selected, sample placed on the measurement stage, and CL images with different accelerating voltages.

References Supporting Information

[65] J. M. Dallesasse, N. El-Zein, N. Holonyak, Jr., K. C. Hsieh, R. D. Burnham, R. D. Dupuis, *J. Appl. Phys.* **1990**, *68*, 2235.

[66] A. R. Sugg, E. I. Chen, T. A. Richard, N. Holonyak, Jr., K. C. Hsieh, *Appl. Phys. Lett.* **1993** ,*62*, 1259.

[67] I. Vurgaftman, J. R. Meyer, *J. Appl. Phys*. **2001**, 89, 5815-5875.